International Journal of Refrigeration 106 (2019) 583–591

Contents lists available at ScienceDirect

International Journal of Refrigeration

journal homepage: www.elsevier.com/locate/ijrefrig

Analysis of refrigerant pipe pressure drop of a CO_2 air conditioning unit for vehicles

Christoph Subei*, Gerhard Schmitz

Institute of Engineering Thermodynamics, Hamburg University of Technology, Denickestr. 17, Hamburg 21073, Germany

ARTICLE INFO

Article history:
Available online 12 April 2019

Keywords:
Air conditioning
R744
Pressure drop
Piping

ABSTRACT

This study investigates the pressure drop in refrigerant pipes of a CO_2 automotive air conditioning unit. A test rig to measure the pressure drop of arbitrarily shaped pipes is presented. As boundary conditions at the inlet of the test section, mass flow, pressure and enthalpy of the refrigerant are independently adjustable to values that cover the whole operating range of a CO_2 automotive air conditioning system for cars in the premium segment. Numerical analysis using CFD and a one-dimensional modelling tool is carried out. The pressure drop for the suction pipe reaches values of up to 500 mbar. CFD simulation predicts the pressure drop with an error of 25.7% for single-phase flow whereas the deviation using one-dimensional models is 46.5%. During two-phase flow the error increases to 55.8% with one-dimensional models and 42.4% using CFD.

Analyse de la chute de pression dans la conduite de frigorigène d'une unité de conditionnement d'air au CO_2 pour des véhicules

Mots-clés: Conditionnement d'air; R744; Chute de pression; Tuyauterie

1. Introduction

Since the environmental impact of refrigerants has become known, the air conditioning and refrigeration sector has been looking for ways to achieve more environmentally friendly air conditioning. The use of so-called natural refrigerants with no Ozone Depleting Potential (ODP) and a low Global Warming Potential (GWP) has been the focus of research and development over the last few years. Technological developments are also influenced by legal requirements. According to the EU directive 2006/40/EG (EU, 2006) the use of the refrigerant R134a is not allowed in new passenger cars because of its high Global Warming Potential (GWP = 1430). Hence, the automotive industry is investigating alternative refrigerants. One option is the use of carbon dioxide (R744) with a GWP value of 1. Additionally, CO_2 is non-toxic, non-flammable and it has a high volumetric capacity. CO_2 has a long history as a refrigerant and according to Bodinus (1999) it was widely used on ships until the 1930s. The critical point of CO_2 is at 304.13 K and 73.7 bar. Therefore, refrigeration units working with CO_2 need to be operated in a supercritical state when the ambient temperature is higher than the critical temperature because the heat rejection takes place at pressures higher than critical pressure. Because of the high system pressure the use of CO_2 declined significantly when the synthetical refrigerants (HCFCs and HFCs) came onto the market. But with the research by Lorentzen and Pettersen (1993) and Lorentzen (1994) in the 1990s, CO_2 is again being considered as an alternative for mobile air conditioning systems. Kim (2004) gives a good overview of system design issues, control strategies and application areas of transcritical CO_2 cycles. With the increased interest in electrical vehicles, the use of CO_2 becomes even more advantageous because it offers higher system performance compared to synthetical refrigerants when the air conditioning unit is used as a heat pump for cabin heating at cold ambient temperatures (Lee et al., 2012; Wang et al., 2018). In 2015, Daimler (2015) announced that the first series production vehicles are equipped with a CO_2 air conditioning unit.

* Corresponding author.
E-mail address: christoph.subei@tuhh.de (C. Subei).

https://doi.org/10.1016/j.ijrefrig.2019.04.005

Nomenclature

d	diameter (m)
Fr	Froude number
g	gravity (m s^{-2})
K	roughness (m)
l	length (m)
$\dot{m}$	mass flow rate (kg s^{-1})
p	pressure (bar)
Re	Reynolds number
T	temperature (K, °C)
u	velocity (m s^{-1})
We	Weber number
x	vapour quality

Greek symbols

ζ	resistance coefficient
η	dynamic viscosity (Pa s^{-1})
λ	thermal conductivity (W m^{-1} K^{-1})
ρ	density (kg m^{-3})
σ	surface tension (N m^{-1})
Φ^2	two-phase friction multiplier

Subscripts

CO_2	carbon dioxide
eq	equivalent
exp	experimental
g	gas
g0	two-phase mixture as gas
i	inner
l	liquid
l0	two-phase mixture as liquid
o	outer
sim	simulated
tp	two-phase

Abbrevations

COP	Coefficient Of Performance
HCFC	Hydrochlorofluorocarbon
HFC	Hydrofluorocarbon
GWP	Global Warming Potential
MARD	Mean Absolute Relative Deviation
m. v.	measured value
ODP	Ozone Depletion Potential
VOF	Volume Of Fluid

One-dimensional modelling approaches are widely used for the numerical design and optimisation of vapour-compression cycles, whereas investigations of local phenomena in individual components like the compressor, evaporator and condenser are carried out using the CFD method. Stevanovic and Hrnjak (2017) present a three-dimensional analysis of oil retention in an evaporator of an automotive air conditioning system. They validate their results against measured values and state that the area where the oil retains can be predicted with higher accuracy than with one-dimensional models. Xu and Hrnjak (2018) use CFD simulation for the investigation of formation, distribution and movement of oil droplets at the discharge valve of a compressor and validate the results against visualisation results. They state that CFD simulation can qualitatively predict the droplet size distribution. Carluccio et al. (2005) examine heat transfer and pressure drop in a cross-flow compact heat exchanger used to cool high-pressure oil in hydraulic circuits of industrial vehicles. With the CFD method, they analyse different fin geometries on the oil side and on the air side. The error of their results is in a range of ±20% compared to literature correlations for the heat transfer and pressure drop in compact heat exchangers with offset strip fins. When considering larger systems or larger time scales such as a drive cycle, the numerical effort of CFD tools is too high. To reduce computational effort, Starace et al. (2018) use the hybrid method for the design of plate-finned tube evaporators. Since the three-dimensional geometric information is considered, the local pressure losses on the refrigerant side and on the air side can be predicted. In addition, the wall temperature distribution, the refrigerant vapour quality and the area with the highest heat transfer rate are determined and used for system optimisation. Li et al. (2017) use a segment-by-segment model based on literature correlations for the pressure drop and heat transfer in channels to investigate an integrated fin and micro-channel gas cooler for a CO_2 automotive air conditioning unit. They state that the heat capacity is predicted within 5% and refrigerant-side pressure drop within 8% deviation from the experimental data. Daviran et al. (2017) compare the performance of the refrigerants R1234yf and R134a in automotive air conditioning systems using a programme code written in Matlab. Heat transfer and pressure drop correlations for straight channels are used for the condenser and for the evaporator. The piping between the components is neglected.

Beside these in-house modelling approaches, there are commercial tools for the design and optimisation of air conditioning systems. Pfafferott and Schmitz (2004) develop a precursor version of the *AirConditioning Library* in the programming language Modelica and simulate a CO_2 refrigeration cycle for aircraft applications. The same tool is used by von Manstein et al. (2017) to investigate different automotive air conditioning concepts for mechanically and electrically driven systems. Both studies use straight pipe models for the connection of the components. Galindo et al. (2016) model an organic-rankine cycle for waste heat recovery from an internal combustion engine using the one-dimensional simulation platform AMESim. For the pressures and temperatures in the cycle they obtain a maximum deviation of 4% compared to experimental values during steady state operating points. Straight pipe models for tubes and channels are used for the piping.

Huang et al. (2016) analyse a model predictive controller to enhance the energy efficiency of an experimental automotive air conditioning system using R134a. To do so, they created a system model in Matlab/Simulink. They state that the impact of the refrigerant pipes with regard to heat transfer and pressure drop can be neglected because of the small pipe length. Li et al. (2011) present an experimental setup to investigate the refrigerant migration in an R134a automotive air conditioning system during shut-down and start-up operations. The test rig comprises adapted refrigerant pipes equipped with ball valves instead of the pipes used in the real automotive application. Thus, their experimental setup as well as their system simulation, performed with the Matlab/Simulink toolbox Thermosys, does not include refrigerant pipes.

Due to the tightly-packed arrangement of components in the engine compartment, refrigerant pipes contain a large number of bends, contractions and expansions. Additionally, some pipes contain a flexible hose to decouple the components mounted on the engine from the components mounted on the chassis. With the use of CO_2 as a replacement for HFC and HFCF refrigerants, hose materials must be redesigned due to high CO_2 diffusion through the rubber which is commonly used. Metallic corrugated tubes are one alternative, but a higher pressure drop due to the surface structure is expected. As a further constraint, pipe diameter should be minimised to keep the filling volume of the refrigerant unit as low as possible, since pipes in automotive air conditioning systems can have a length of up to 2 m.

The objective of this paper is a detailed experimental and numerical analysis of the pressure drop in two differently-shaped

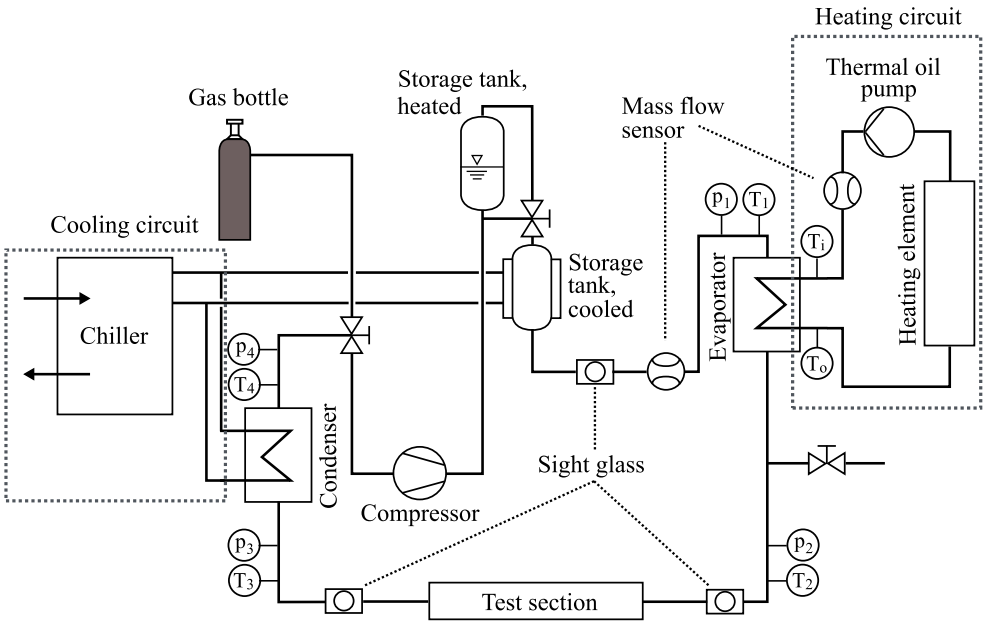

Fig. 1. Schematic of the test rig.

Table 1
Operating range of the test rig.

Parameter	Operating range
Pressure	30 bar to 130 bar
Temperature	−20 °C to 130 °C
Mass flow rate	30 kg h^{-1} to 250 kg h^{-1}

refrigerant pipes, using CO_2 as the working fluid. The literature overview shows that refrigerant pipes have been either neglected or modelled as straight pipes throughout the studies performed so far. In this study, a generic pipe consisting of an interconnection of 90° bends, a helical coil and straight pipe sections is analysed. In addition, a suction pipe connecting the internal heat exchanger and the compressor inlet from an automotive air conditioning unit is investigated. The purpose of this study is the detailed comparison of experimental data with numerical results of a one-dimensional modelling approach as well as a three-dimensional simulation. From the results it can be estimated whether or not the pipe pressure drop has an impact on system behaviour.

2. Experimental setup and data processing

2.1. Test rig

The schematic of the high-pressure test rig used for the analysis of pipe pressure drop is shown in Fig. 1. There are three main loops: the high-pressure loop filled with CO_2 and the heating and the cooling circuit, which are filled with thermal oil to supply condenser and evaporator. Instead of building up a vapour compression cycle, the test rig is constructed as a pump circuit. The advantage of this setup is that all operating conditions of a CO_2 automotive air conditioning system can be adjusted at the inlet of one test section (p_2, T_2). Depending on the mounting location in the air conditioning unit, the refrigerant flows through the refrigerant pipes in either a superheated gas state, subcooled liquid state or two-phase mixture state. With the operating range of the test rig as indicated in Table 1, the operating conditions of a CO_2 refrigeration system for cars in the premium and luxury car segment can be simulated.

An air-driven compressor (Maximator, Type DLE-15) is used as the recirculation unit, which is able to pump CO_2 in a liquid, gas and two-phase state. This compressor is a very robust reciprocating compressor without lubrication. Lubricating oil has a considerable influence on pressure drop, which is not part of this study, but intensively discussed in literature for straight pipe flow (Weise et al., 2017; Wetzel et al., 2014). The disadvantage of this compressor is the resulting pulsation. The stroke rate of the compressor is in the range of 20 min^{-1} to 90 min^{-1}.

During stationary operation the recirculation unit is fed with subcooled liquid refrigerant from the condenser. Two storage tanks are installed behind the compressor. One storage tank can be heated to control the pressure in the test rig by the volume of the gas cushion in this storage tank. The second storage tank was installed to reduce the pulsations, but the effect of this dampening unit is too small to dampen the pulsations of the reciprocating compressor completely.

Behind the mass flow sensor, the refrigerant enters a plate heat exchanger where it can be heated up, or be either partially or fully evaporated. The outlet enthalpy of CO_2 is calculated by an energy balance based on the mass flow rate and temperature of the thermal oil and the inlet enthalpy of the CO_2. The heat exchanger is insulated with insulation material ($\lambda = 0.038\,W\,m^{-1}\,K^{-1}$) with a thickness of 13 mm. At the inlet and at the outlet of the test section, a sight glass is installed to visually check the phase state of the fluid. For two-phase inlet conditions the flow pattern can be estimated, but not reliably determined. In the test section, arbitrarily shaped pipes can be installed using a flange connection. Behind the sight glass, a settling section is installed with a length of 1 m. The pipe diameter of the settling section is chosen according to the inlet diameter of the installed pipe. The pressure drop in the test section is measured by a differential pressure sensor (WIKA DPT-10) with an adjustable operating range from 0 bar to 4 bar and an accuracy of ±0.15% of the adjusted scale. The operating range of the sensor is adapted to the expected pressure drop. The differential pressure pipes have a diameter of 1/8″. The pipe routing between junction and sensor increases monotonically.

Behind the test section, CO_2 is condensed in a plate heat exchanger. The temperature of the fluid at the condenser outlet is used for the fine-tuning of the system pressure. The test rig is able

Table 2
Instrumental and calibrated uncertainties.

Parameter	Instrument	Range	Uncertainty
Pressure	WIKA Typ A 10	0 bar to 160 bar	± 1% of the scale
Differential pressure	WIKA DPT-10	0 bar to 4 bar	± 0.15% of the scale
Temperature	WIKA Typ TR40	−196 °C to 600 °C	± 0.2 K
Mass flow rate	SITRANS FC Mass 2100	0 kg h^{-1} to 300 kg h^{-1}	± 1% of m. v.
Mass flow rate	Heinrichs TME-S90	0 kg h^{-1} to 3000 kg h^{-1}	± 1.5% of m. v.
Heat flux evaporator		0 kW to 24 kW	± 5%
Enthalpy test section inlet			± 5 kJ kg^{-1}

to operate at temperatures between −20 °C and 130 °C, which correspond with the minimum temperature of the chiller (−20 °C) and the maximum temperature in the heating circuit (130 °C). The thermal capacity of the chiller and the heating unit is 24 kW.

2.2. Data processing

A National Instruments data acquisition system, along with a LabView data processing programme is used to acquire the measurement data. The raw data is saved and evaluated with Matlab. All measurement values are recorded with a frequency of 2 Hz. Steady state condition is achieved when the values for temperature, pressure and mass flow rate at the inlet of the test section do not vary by more than 0.5% for at least 5 min. After that, measurement values are taken for at least 5 min and averaged for the evaluation of stationary operating points. The system pressure is monitored by 7 pressure transducers in the cycle with an accuracy of ± 1% of full scale. Temperature measurements are taken with calibrated Pt100 sensors with an accuracy of ± 0.2 K after calibration. For the evaluation of refrigerant properties, the LabView programme as well as the Matlab evaluation routines are linked to the property calculation software CoolProp (Bell et al., 2014).

Validation of the pressure drop measurement is performed with a straight horizontal pipe with an inner diameter of 8 mm and a length of 3.2 m. A comparison with the Colebrook equation (Eq. (2)) gives a mean error of 4.6%. The pipes are insulated during these validation experiments as well as during the experiments with the refrigerant pipes. Thus, heat losses to the environment can be neglected and the pipes can be considered as adiabatic.

2.3. Uncertainty analysis

For the uncertainty analysis, the known accuracy of the sensors for mass flow and pressure measurements are taken into account according to Table 2. The temperature sensors are calibrated according to the method described in JCGM (2010) and for further evaluation the calibrated accuracy is taken into consideration. For the uncertainty of the enthalpy of the fluid at the inlet of the test section, the uncertainties of the mass flow measurements of thermal oil and CO_2 are taken into account as well as the temperature measurements of the thermal oil at the inlet and outlet of the evaporator and the temperature measurement of the CO_2 at the inlet of the evaporator.

3. Pressure drop in refrigerant pipes

3.1. Pipe geometry

For the analysis of refrigerant pipe pressure drop, two different pipe geometries are investigated in this study. Fig. 2 shows the CAD data of a pipe consisting of multiple 90° bends, straight pipe sections and a helical coil. The pipe has an inner diameter of d_i = 6 mm and an outer diameter of d_o = 8 mm. The unwound length, also referred to as the equivalent length of a straight pipe, is l_{eq} = 1.31 m. The pipe material is stainless steel with a surface roughness of $K = 3\,\mu m$ determined with an optical measuring method. The pipe can be divided into several bent and straight pipe sections. Table A.1 in the Appendix contains detailed dimensions for each of these parts. This data is used for the one-dimensional system model built from 90° bend and straight pipe models as shown in Fig. 2. The helical coil is represented by four 90° bend models.

Fig. 3 shows a suction pipe of a CO_2 automotive air conditioning unit which connects the internal heat exchanger and the compressor. The unwound length of the pipe is l_{eq} = 1.09 m. The inner diameter of the metal part is d_i = 8 mm and the outer diameter is d_o = 10 mm. At the transition to the hose part a cross-sectional change occurs and the inner diameter increases to d_i = 10 mm and the outer diameter to d_o = 12 mm. The pipe is divided into several parts consisting of bent and straight pipe sections with the dimensions as given in Table A.2 in the Appendix. The part numbers correspond to Fig. 3 where the one-dimensional model is shown. The metal part of the pipe is made of aluminium with a surface roughness of $K = 6\,\mu m$. A detailed surface roughness of the hose part cannot be determined by optical methods. On the inner side of the hose part a Teflon layer is in contact with the refrigerant. Outer layers vary and consist of rubber materials partially reinforced with metal. The Teflon layer on the inner side leads to a smooth surface. Therefore, surface roughness for this part is neglected during simulation.

3.2. Single-phase flow

Fig. 4 contains the experimental results for the pipe shown in Fig. 2. The experimental pressure drop is obtained during mass flow variation at inlet pressures of 35 bar and 100 bar and temperatures of 10 °C and 70 °C. For comparison with the procedure frequently used in literature of assuming a straight pipe, the pressure drop is calculated based on the Colebrook equation (VDI, 2010):

$$\Delta p = \zeta\,(\mathrm{Re})\,\frac{l_{eq}}{d_i}\,\frac{\rho u_i^2}{2} \tag{1}$$

$$\frac{1}{\sqrt{\zeta}} = -2\log\left[\frac{2.51}{\mathrm{Re}_i\sqrt{\zeta}} + \frac{K/d_i}{3.71}\right] \tag{2}$$

For a comparison of experimental data with calculated pressure drop values the Mean Absolute Relative Deviation (MARD)

$$\mathrm{MARD} = \frac{1}{N}\sum\left|\frac{y_{pred}(i) - y_{exp}(i)}{y_{exp}(i)}\right| \cdot 100 \tag{3}$$

and the percentage of data within ± 30% of the experimental results are considered. The MARD for the measurement series at 35 bar is 34.9% and therefore slightly higher compared to 30.6% at 100 bar. As the Colebrook equation does not capture any additional pressure drop due to the curved parts, it is consistent that the calculated pressure drop is smaller in comparison to the experimental values.

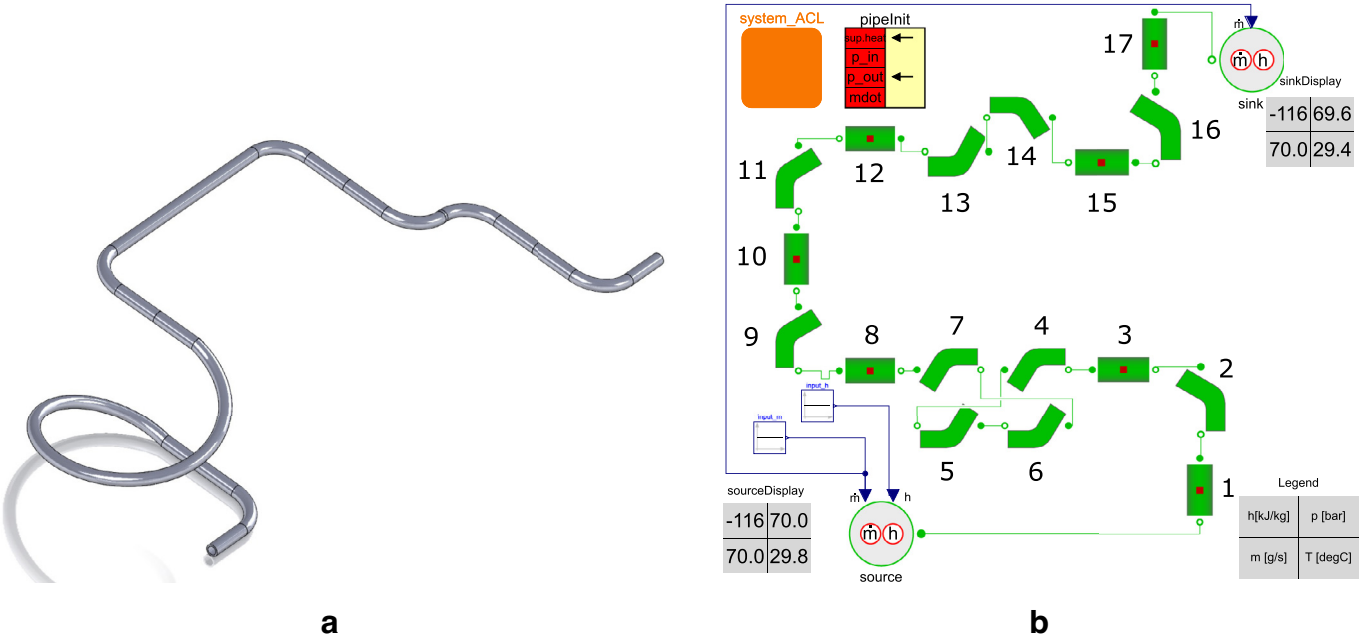

Fig. 2. Interconnection of multiple 90° bends and a helical coil as a CAD model (a) and built from one-dimensional bend and straight pipe models (b).

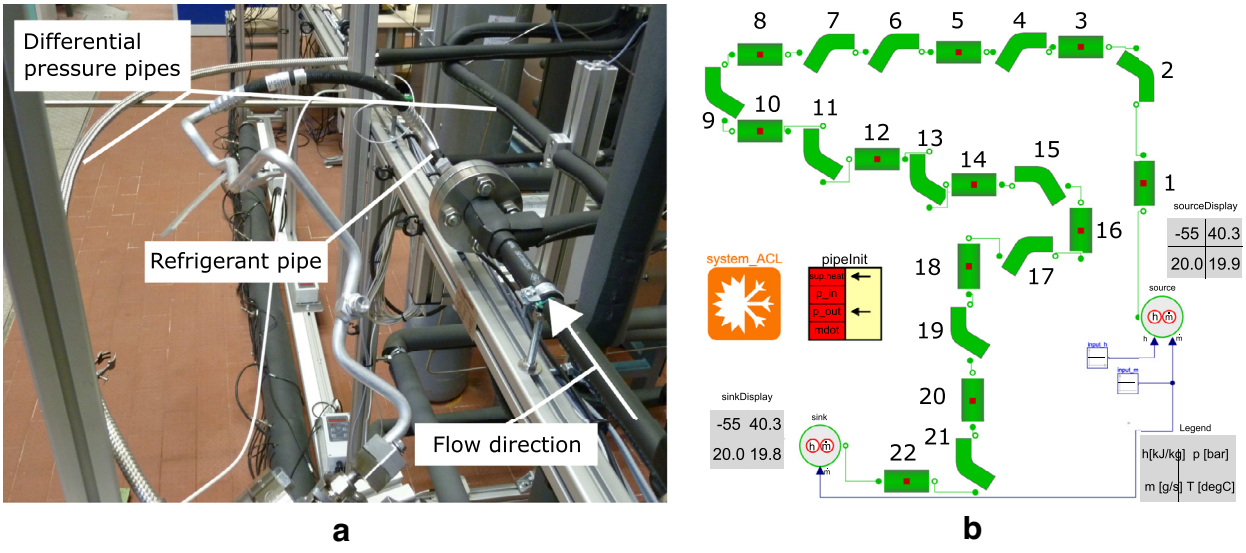

Fig. 3. Suction pipe of a CO_2 automotive air conditioning system installed in the test-rig (a) and built from one-dimensional bend and straight pipe models (b).

Fig. 5 shows similar results for the pressure drop of the suction pipe. Experimental pressure drop is given as a function of mass flow rate at inlet pressures of 40 bar and 51 bar with temperatures of 20 °C and 34 °C. Due to the assembly position between internal heat exchanger and compressor, the inlet phase state of the refrigerant into a suction pipe is gaseous. When using CO_2 in automotive air conditioning units, the pressure varies between 35 bar and 50 bar and the temperature varies between 10 °C and 35 °C. The deviation between the straight pipe pressure drop and the experimental results amounts to 59.7% and 60.5%. Thus, the MARD is significantly higher than for the interconnection pipe. Although the larger inner diameter of the hose part is taken into account in this comparison, the pressure drop due to the cross-section expansion cannot be captured during simplified calculation with the Colebrook equation. Experimental results for both pipes show that the process of assuming a straight pipe underestimated the pressure drop significantly.

The pressure drop for both pipes is calculated numerically with the CFD tool Star-CCM+ and with one-dimensional pipe models available in the Modelica *AirConditioning Library* using the simulation environment Dymola 2018 FD01. Mass flow, pressure and temperature are implemented as boundary conditions at the inlet of the simulation, according to the experimental data. The wall boundary condition is set to adiabatic because the pipe is insulated during the experiments, and the surface roughness of the pipe wall is set to values for aluminium and stainless steel as given in Section 3.1.

For the pressure drop calculation, the straight pipe model of the *AirConditioning Library* utilises the Colebrook equation. The bend model uses experimentally determined resistance coefficients from Idelcik and Ginevski (2007) which are implemented as a function of pipe diameter and bend radius.

In the CFD simulation, a constant density model is used along with a gas model, where the fluid properties are defined. The

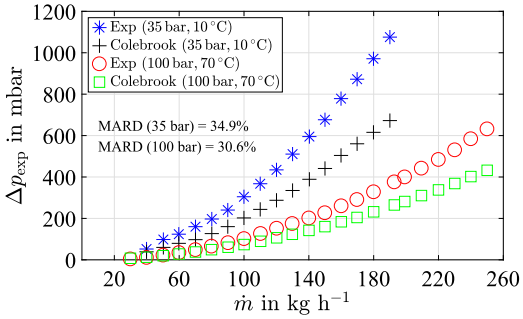

Fig. 4. Pressure drop at different mass flow rates for the interconnection pipe and for a straight pipe with equivalent length at different inlet boundary conditions.

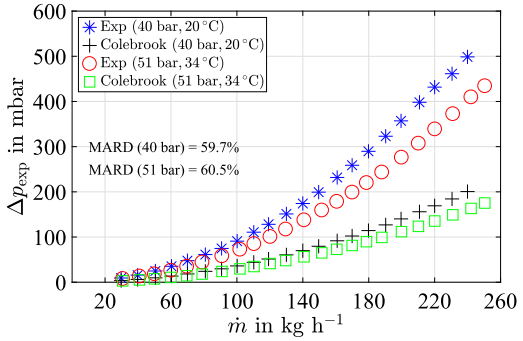

Fig. 5. Pressure drop at different mass flow rates for the suction pipe and for a straight pipe with equivalent length at different inlet boundary conditions.

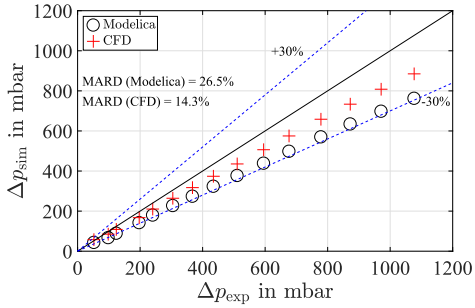

Fig. 6. Numerically calculated pressure drop using CFD and Modelica compared to experimental data for the interconnection pipe at $p = 35$ bar and $T = 10$ °C.

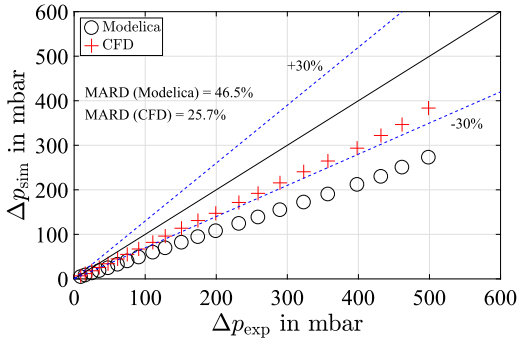

Fig. 7. Numerically calculated pressure drop using CFD and Modelica compared to experimental data for the suction pipe at $p = 40$ bar and $T = 20$ °C.

outlet is set to pressure outlet. The gravity model is activated and a straight section before the inlet ensures a developed flow profile. The wall boundary condition is set to adiabatic and the surface roughness is considered. Because of the high Reynolds number ($\mathrm{Re} \geq 10,000$) the flow is fully turbulent. The $k-\epsilon$ turbulence model with a high y+ wall treatment is used. Hence, a wall function is used to model the physics of the boundary layer instead of resolving the boundary layer completely. The mesh is therefore constructed with two prism layers and the y+ value is monitored to make sure that the values are above 30, which is the lower limit for which the model is suitable. In a grid independence study, the pressure drop is evaluated for five refined meshes with cell numbers from 0.3 million to 5.1 million. A structured grid with hexahedron cells is used. With a total cell number of 2.3 million for the interconnection pipe and with 2.8 million cells for the suction pipe, the change in the calculated pressure drop is below 1% when compared to a larger number of cells, and therefore the result can be regarded as grid-independent. The simulation uses the segregated flow solver, and since no transient processes occur, the steady flow model is chosen.

Fig. 6 compares the simulated pressure drop to the experimental values for the interconnection pipe at $p = 35$ bar and $T = 10$ °C. As the Modelica model contains bend and straight pipe models, an improvement compared to utilising the Colebrook equation with equivalent length is achieved, resulting in a lower MARD of 26.5%. The serial connection of bends leads to non-developed flow profiles in the downstream components. Resistance coefficients in literature as they are used in one-dimensional modelling approaches are experimentally determined with a developed flow profile. Hence, the Modelica model has a greater deviation from the experimental values compared to CFD simulation, where the flow profile is resolved in all spatial directions. The CFD simulation shows a MARD of 14.3%, which can possibly be attributed to an error in determining the surface roughness, since the deviation is comparable in all points.

Fig. 7 shows that the pressure drop calculated with CFD methods is 25.7% lower than the measured values for the suction pipe. Using the one-dimensional modelling approach as shown in Fig. 3 leads to a MARD of 46.5%. Both simulation methods show a larger error compared to the first pipe. As the suction pipe is manufactured for real application in a vehicle and not for scientific purposes, tolerances for the dimensions of the curved parts are not strict. Most of the bends are flattened resulting in a non-circular cross-section. The change in diameter at the transition between metal part and hose part leads to an additional pressure drop which is not considered in the Modelica model. The simulated pressure drop at all points is smaller than the experimental values, which indicates a systematic error like a too low value for the surface roughness. Especially for the hose part, the assumption of a smooth surface may not be justified. Under the high pressure, the Teflon layer can be pressed into the structure of the outer layers consisting of different rubber materials, partially reinforced with metal.

It turns out that the calculation with CFD already represents a considerable improvement compared to the current procedure of considering pressure drop in a straight pipe with equivalent length. But for refrigerant pipes of an automotive air conditioning unit, there is still a significant difference between the simulated values and the experimental results. Therefore, the pipes have to be analysed experimentally to obtain reliable resistance coefficients which can be used for improving the system simulation.

3.3. Two-phase flow

Although most refrigerant pipes are flowed through in a single-phase state, some of the pipes contain refrigerant in two-phase flow. For straight pipe flow, a large number of experimental analyses can be found in literature containing different flow patterns, different saturation pressures and inlet vapour qualities as well as

adiabatic and diabatic wall boundary conditions (Charnay et al., 2015; Xu et al., 2012). The pressure drop is a function of steam quality and increases with higher steam quality until a maximum pressure drop is reached around a value of $x = 0.8$. With a steam quality higher than 0.8, the pressure drop decreases until the refrigerant is completely evaporated and in a superheated gas phase. In addition to the interaction between fluid and wall, which leads to pressure losses due to the friction forces, there are further friction effects because of the interactions at the boundary of the two phases, due to the different flow velocity of the two phases. This additional friction explains the maximum of the pressure drop at higher qualities. New pressure drop prediction methods take the flow pattern into account (Mastrullo et al., 2012). For CO_2 Cheng et al. (2008) published a flow pattern map based on experimental results in straight pipes. For the quality range of around 0.8 an annular flow occurs according to this flow pattern map. In the case of annular flow, there is a large interface between the two phases which causes higher friction. At a quality of 0.9 or higher the flow pattern changes to a dry-out flow where small liquid droplets are entrained with the flow. In this case the pressure drop is dominated by the interaction of the fluid with the wall.

For the experimental analysis of pipe pressure drop in a two-phase state, the enthalpy of the refrigerant at the inlet of the test section is controlled based on a heat balance around the evaporator as shown in Fig. 1. For the calculation of two-phase pressure drop, one approach is the two-phase multiplier method. Thereby, the pressure drop of the single-phase flow either in a pure liquid or pure gas phase state is multiplied by a factor Φ^2 called two-phase multiplier:

$$\Delta p_{\mathrm{tp}} = \Phi^2_{\mathrm{l,g}}\, \Delta p_{\mathrm{l,g}} \tag{4}$$

The Friedel correlation is used for comparison with straight pipe flow:

$$\Phi^2_{\mathrm{l}} = (1-x)^2 + x^2\left(\frac{\rho_{\mathrm{l}}\zeta_{\mathrm{g}}}{\rho_{\mathrm{g}}\zeta_{\mathrm{l}}}\right) + 3.43x^{0.685}(1-x)^{0.24}\left(\frac{\rho_{\mathrm{l}}}{\rho_{\mathrm{g}}}\right)^{0.8} \times \left(\frac{\eta_{\mathrm{g}}}{\eta_{\mathrm{l}}}\right)^{0.22}\left(1-\frac{\eta_{\mathrm{g}}}{\eta_{\mathrm{l}}}\right)^{0.89}\mathrm{Fr}_{\mathrm{l0}}^{-0.047}\mathrm{We}_{\mathrm{l0}}^{-0.0334} \tag{5}$$

with

$$\zeta_{\mathrm{l,g}} = \begin{cases} \frac{64}{\mathrm{Re}_{\mathrm{g0,l0}}} & \mathrm{Re}_{\mathrm{g0,l0}} \le 1055 \\ \left[0.86859 \ln\left(\frac{\mathrm{Re}_{\mathrm{g0,l0}}}{1.964\ln \mathrm{Re}_{\mathrm{g0,l0}} - 3.8215}\right)\right]^{-2} & \mathrm{Re}_{\mathrm{g0,l0}} > 1055 \end{cases}$$

and

$$\mathrm{Fr}_{\mathrm{l0}} = \frac{\dot{m}^2}{g d_{\mathrm{i}} \rho_{\mathrm{l}}^2} \tag{6}$$

$$\mathrm{We}_{\mathrm{l0}} = \frac{\dot{m}^2 d_{\mathrm{i}}}{\rho_{\mathrm{l}}\sigma} \tag{7}$$

The Friedel correlation is based on experimental values for the refrigerant R22 (Friedel, 1979).

Fig. 8 shows the experimental pressure drop for different inlet qualities for the interconnection pipe. The mass flow rate is set to a constant value of 125 kg h^{-1} at pressures of 35 bar and 60 bar. The Friedel correlation is evaluated using the equivalent pipe length of $l_{\mathrm{eq}} = 1.31$ m. The measured series at 35 bar shows a peak in pressure drop at a vapour quality of 0.8. The MARD of the Friedel correlation is 43.6% as it does not capture the peak behaviour of the pressure drop. At a higher pressure of 60 bar the peak is not observable because of the smaller difference in fluid properties of the gas and the liquid phase. The Friedel correlation fits the data with a MARD of 26.9%.

In Fig. 9, a similar comparison is performed for the suction pipe at 30 bar and 50 bar and a mass flow rate of 125 kg h^{-1}. Again there is a peak in the pressure drop at a quality of 0.8 at the lower

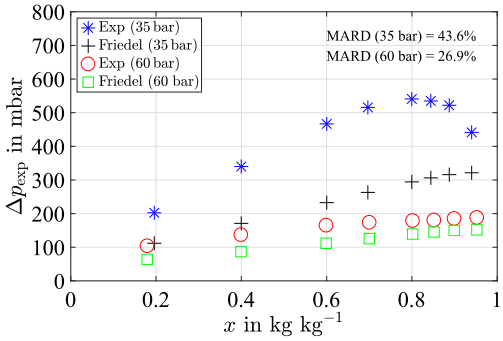

Fig. 8. Pressure drop at different inlet qualities for the interconnection pipe and for a straight pipe using the Friedel equation with equivalent length.

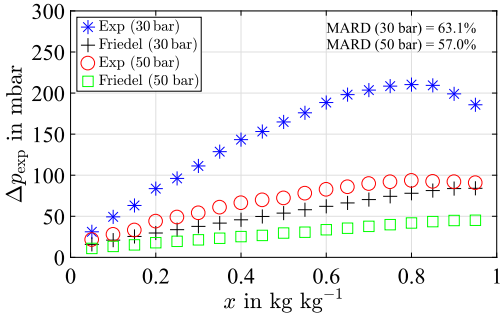

Fig. 9. Pressure drop at different inlet qualities for the suction pipe and for a straight pipe using the Friedel equation with equivalent length.

pressure. At 50 bar this peak is smaller, but still observable. Assuming a straight pipe with equivalent length leads to a significant deviation compared to experimental results. The MARD for both pressures is in the same range and amounts to 63.1% and 57.0%, respectively.

In the CFD setup a Volume Of Fluid (VOF) approach is chosen for the modelling of the two-phase flow. Thus, distinct Eulerian phases are defined for the gas and for the liquid phase. For the fluid properties, the values for the pure liquid and pure gas phase in a saturated state at the inlet pressure are taken from CoolProp. The inlet boundary conditions for pressure, quality and mass flow rate are taken from the experiments. The $k-\epsilon$ turbulence model with a high y+ wall treatment is used. The wall boundary conditions are set to adiabatic and the surface roughness is taken into account. The same mesh type and the same total number of cells are used as in the single-phase flow simulation. Segregated solver is chosen for the numerical solution.

The straight pipe model of the *AirConditioning Library* uses the Friedel correlation for pressure drop calculation. The bend model setup is the same as for the single-phase flow simulation since the models do not include any correlation for two-phase flow.

Fig. 10 depicts the simulated pressure drop for the interconnection pipe. It can be determined that the Modelica model has a MARD of 44.9% which is nearly the same as if modelling the pipe as a straight pipe with equivalent length, although the Modelica model uses the bend models for the curved parts. But since these models use resistance coefficients obtained for single-phase flow, the pressure drop is underestimated. The fluid-fluid interaction, responsible for an additional pressure drop, is not taken into account. The MARD of the CFD model amounts to 35.0% and significantly exceeds the deviation between numerical and experimental results of the same pipe for single-phase flow. The reason is the neglection of the flow pattern again. The VOF model is able to track the interface between two phases, but since the flow pattern at the inlet of

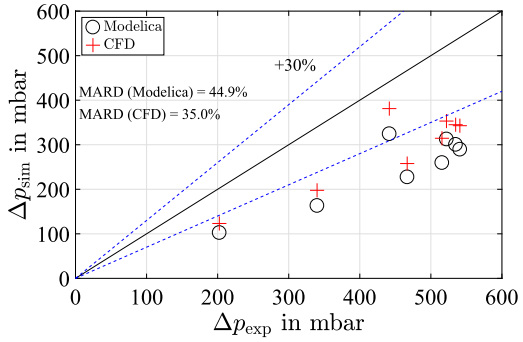

Fig. 10. Numerically calculated pressure drop using CFD and Modelica compared to experimental data for the interconnection pipe at $p = 35$ bar and $\dot{m} = 125$ kg h^{-1}.

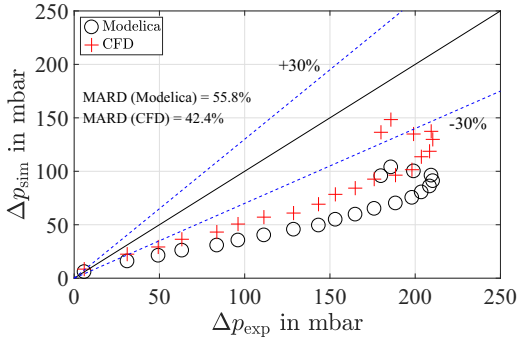

Fig. 11. Numerically calculated pressure drop using CFD and Modelica compared to experimental data for the suction pipe at $p = 30$ bar and $\dot{m} = 125$ kg h^{-1}.

the pipe is unknown, the volume fraction has the same value over the entire cross-section and no phase separation is observable.

The MARD between the CFD model and experiments for the suction pipe is 42.4% as shown in Fig. 11. This is mainly due to the peak behaviour of the pressure drop at higher qualities, which cannot be covered with the CFD model. Therefore, the deviation at vapour qualities around 0.8 is greater compared to lower and higher vapour quality ranges. The one-dimensional modelling approach shows a MARD of 55.8%. As for the interconnection pipe, the deviation is comparable to the calculation of pressure drop in a straight pipe with equivalent length.

The results show that for two-phase flow, both simulation methods have a greater deviation from the experimental results. The main reason is that the flow pattern, which is responsible for a part of the total pressure drop, cannot be captured by these methods. Like in single-phase flow simulation, further reasons for the deviation are inaccuracies in the manufactured pipe and errors due to the direct connection of curved parts which cannot be modelled correctly with one-dimensional bend models.

4. Conclusions

This study covers the analysis of pressure drops in pipes of an automotive air conditioning system using CO_2 as a refrigerant. A test rig for the experimental investigation of pressure drop in arbitrarily shaped pipes is presented. The operating range of the test rig is based on the operating range of an automotive air conditioning unit for premium cars and covers pressures from 30 bar to 130 bar, temperatures from −20 °C to 130 °C and mass flow rates of up to 250 kg h^{-1}. Investigations are carried out for single-phase and two-phase pipe flow. Results for two different pipe geometries are presented. The first pipe is an interconnection of multiple 90° bends, straight pipe sections and a helical coil. The second pipe is a suction pipe of a CO_2 air conditioning system containing a metal part with differently curved bends as well as a flexible hose.

Experimental results are compared to CFD simulation and to the one-dimensional modelling approach consisting of bend and straight pipe models of the Modelica *AirConditioning Library* using Dymola as a solver. The following conclusions are drawn:

- In literature it is common to use straight pipe correlations to consider pipe pressure drop. Deviation compared to experimental pressure drop of the pipes examined in this study is 40% and 60%, indicating that the current procedure considerably underestimates the pressure drop.
- Since the pressure drop for the suction pipe reaches values of up to 500 mbar, refrigerant pipe pressure drop should not be neglected in system simulation.
- Using CFD simulation, the deviation compared to experimental values is considerably lower and the pipe pressure drop can be predicted with an error margin of 14.3% and 25.7% in single-phase flow. In two-phase flow, the deviation is higher because the CFD model used in this study is not able to account for the additional pressure drop caused by phase interaction.
- The modelling of refrigerant pipes as an interconnection of bend and straight pipe models in Modelica only leads to a minor improvement in accuracy. Since the numerical effort increases, and the larger number of models and equations might affect the stability of the numerical solution, this modelling approach should not be chosen.

For future analysis, the pressure drop for the remaining pipes of an automotive air conditioning system should be determined and used for calibrating pipe models to improve system simulation. With these calibrated pipe models, the impact on COP, on compressor shaft power and on evaporator air outlet temperature should be quantified.

Acknowledgement

The authors would like to thank TuTech Innovation GmbH, Hamburg, Germany, for their financial support for this research project.

Appendix A

Table A.1
Dimensions of the parts of the interconnection pipe.

Part no. dimensionless	Length mm	Radius mm	Angle ◦
1	60		
2		30	90
3	100		
4		60	90
5		60	90
6		60	90
7		60	90
8	200		
9		30	90
10	50		
11		30	90
12	90		
13		30	90
14		30	90
15	90		
16		30	90
17	60		

Table A.2
Dimensions of the parts of the suction pipe.

Part no. dimensionless	Length mm	Radius mm	Angle ◦
1	55		
2		25	110
3	60		
4		155	90
5	60		
6		20	110
7		25	90
8	20		
9		35	30
10	30		
11		30	30
12	40		
13		15	40
14	75		
15		15	90
16	75		
17		20	60
18	55		
19		20	80
20	45		
21		20	90
22	55		

References

Bell, I.H., Wronski, J., Quoilin, S., Lemort, V., 2014. Pure and pseudo-pure fluid thermophysical property evaluation and the open-source thermophysical property library CoolProp. Ind. Eng. Chem. Res. 53 (6), 2498–2508. doi:10.1021/ie4033999.

Bodinus, W., 1999. The rise and fall of carbon dioxide systems: the first century of air conditioning. ASHRAE J. 41 (4), 37–42.

Carluccio, E., Starace, G., Ficarella, A., Laforgia, D., 2005. Numerical analysis of a cross-flow compact heat exchanger for vehicle applications. Appl. Therm. Eng. 25 (13), 1995–2013. doi:10.1016/j.applthermaleng.2004.11.013.

Charnay, R., Revellin, R., Bonjour, J., 2015. Discussion on the validity of prediction tools for two-phase flow pressure drops from experimental data obtained at high saturation temperatures. Int. J. Refrig. 54, 98–125. doi:10.1016/j.ijrefrig.2015.02.014.

Cheng, L., Ribatski, G., Moreno J., Thome, J.R., 2008. New prediction methods for CO_2 evaporation inside tubes: Part I – a two-phase flow pattern map and a flow pattern based phenomenological model for two-phase flow frictional pressure drops. Int. J. Heat Mass Transf. 51 (1–2), 111–124. doi:10.1016/j.ijheatmasstransfer.2007.04.002.

Daimler, A.G., 2015. Mercedes-Benz to equip first vehicle models with CO_2 air conditioning systems, Stuttgart. https://www.daimler.com/documents/investors/nachrichten/kapitalmarktmeldungen/daimler-ir-release-en-20151020.pdf (accessed 24.04.2019).

Daviran, S., Kasaeian, A., Golzari, S., Mahian, O., Nasirivatan, S., Wongwises, S., 2017. A comparative study on the performance of HFO-1234yf and HFC-134a as an alternative in automotive air conditioning systems. Appl. Therm. Eng. 110, 1091–1100. doi:10.1016/j.applthermaleng.2016.09.034.

EU (European Union), 2006. Directive 2006/40/EC of the European parliament and of the Council, of 17 May 2006 relating to emissions from air-conditioning systems in motor vehicles and amending Council Directive 70/156/EEC (Text with EEA relevance), Official Journal of the European Union. https://eur-lex.europa.eu/LexUriServ/LexUriServ.do?uri=OJ:L:2006:161:0012:0018:EN:PDF (accessed 24.04.2019).

Friedel, L., 1979. Improved friction pressure drop correlations for horizontal and vertical two phase pipe flow. 3R Int. 18 (7), 485–491.

Galindo, J., Dolz, V., Royo-Pascual, L., Haller, R., Melis, J., 2016. Modeling and experimental validation of a volumetric expander suitable for waste heat recovery from an automotive internal combustion engine using an organic rankine cycle with ethanol. Energies 9 (4), 279. doi:10.3390/en9040279.

Huang, Y., Khajepour, A., Bagheri, F., Bahrami, M., 2016. Modelling and optimal energy-saving control of automotive air-conditioning and refrigeration systems. P. I. Mech. Eng. D J. Aut. 231 (3), 291–309. doi:10.1177/0954407016636978.

Idelcik, I.E., Ginevski, A., 2007. Handbook of Hydraulic Resistance, 4., rev. and augmented ed. Begell House, Redding, Conn..

JCGM (Joint Committee for Guides in Metrology), 2010. Evaluation of measurement data - Guide to the expression of uncertainty in measurement. https://www.bipm.org/utils/common/documents/jcgm/JCGM_100_2008_E.pdf (accessed 24.04.2019).

Kim, M., 2004. Fundamental process and system design issues in CO_2 vapor compression systems. Prog. Energy Combust. Sci. 30 (2), 119–174. doi:10.1016/j.pecs.2003.09.002.

Lee, M.-Y., Lee, H.-S., Won, H.-P., 2012. Characteristic evaluation on the cooling performance of an electrical air conditioning system using r744 for a fuel cell electric vehicle. Energies 5 (5), 1371–1383. doi:10.3390/en5051371.

Li, B., Peuker, S., Hrnjak, P.S., Alleyne, A.G., 2011. Refrigerant mass migration modeling and simulation for air conditioning systems. Appl. Therm. Eng. 31 (10), 1770–1779. doi:10.1016/j.applthermaleng.2011.02.022.

Li, J., Jia, J., Huang, L., Wang, S., 2017. Experimental and numerical study of an integrated fin and micro-channel gas cooler for a CO_2 automotive air-conditioning. Appl. Therm. Eng. 116, 636–647. doi:10.1016/j.applthermaleng.2016.12.140.

Lorentzen, G., 1994. Revival of carbon dioxide as a refrigerant. Int. J. Refrig. 17 (5), 292–301. doi:10.1016/0140-7007(94)90059-0.

Lorentzen, G., Pettersen, J., 1993. A new, efficient and environmentally benign system for car air-conditioning. Int. J. Refrig. 16 (1), 4–12. doi:10.1016/0140-7007(93)90014-Y.

von Manstein, A., Limperich, D., Banakar, S., 2017. Simulative comparison of mobile air-conditioning concepts for mechanical and electrical driven systems. Proceedings of the 12th International Modelica Conference (2) 783–790. doi:10.3384/ecp17132783.

Mastrullo, R., Mauro, A.W., Thome, J.R., Toto, D., Vanoli, G.P., 2012. Flow pattern maps for convective boiling of CO_2 and R410A in a horizontal smooth tube: experiments and new correlations analyzing the effect of the reduced pressure. Int. J. Heat Mass Transf. 55 (5–6), 1519–1528. doi:10.1016/j.ijheatmasstransfer.2011.11.003.

Pfafferott, T., Schmitz, G., 2004. Modelling and transient simulation of CO2-refrigeration systems with Modelica. Int. J. Refrig. 27 (1), 42–52. doi:10.1016/S0140-7007(03)00098-7.

Starace, G., Fiorentino, M., Meleleo, B., Risolo, C., 2018. The hybrid method applied to the plate-finned tube evaporator geometry. Int. J. Refrig. 88, 67–77. doi:10.1016/j.ijrefrig.2017.12.007.

Stevanovic, V.D., Hrnjak, P., 2017. Numerical simulation of three dimensional two-phase flow and prediction of oil retention in an evaporator of the automotive air conditioning system. Appl. Therm. Eng. 117, 468–480. doi:10.1016/j.applthermaleng.2017.02.027.

VDI (Ed.), 2010. VDI Heat Atlas. Springer Berlin Heidelberg, Berlin, Heidelberg.

Wang, D., Yu, B., Hu, J., Chen, L., Shi, J., Chen, J., 2018. Heating performance characteristics of CO_2 heat pump system for electrical vehicle in a cold climate. Int. J. Refrig. 85, 27–41. doi:10.1016/j.ijrefrig.2017.09.009.

Weise, S., Wetzel, M., Dietrich, B., Wetzel, T., 2017. Influence of fully miscible lubricating oil on the pressure drop during flow boiling of CO_2 inside an enhanced tube. Exp. Therm Fluid Sci. 81, 223–233. doi:10.1016/j.expthermflusci.2016.09.018.

Wetzel, M., Dietrich, B., Wetzel, T., 2014. Influence of oil on heat transfer and pressure drop during flow boiling of CO_2 at low temperatures. Exp. Therm Fluid Sci. 59, 202–212. doi:10.1016/j.expthermflusci.2014.05.001.

Xu, J., Hrnjak, P.S., 2018. Formation, distribution, and movement of oil droplets in the compressor plenum. Int. J. Refrig. 93, 184–194. doi:10.1016/j.ijrefrig.2018.06.020.

Xu, Y., Fang, X., Su, X., Zhou, Z., Chen, W., 2012. Evaluation of frictional pressure drop correlations for two-phase flow in pipes. Nucl. Eng. Des. 253, 86–97. doi:10.1016/j.nucengdes.2012.08.007.